Avalanches in the weakly driven Frenkel-Kontorova model

Franz-Josef Elmer
Institut für Physik, Universität Basel, CH-4056 Basel, Switzerland
(Received 6 April 1994)

A damped chain of particles with harmonic nearest-neighbor interactions in a spatially periodic, piecewise harmonic potential (Frenkel-Kontorova model) is studied numerically. One end of the chain is pulled slowly, which acts as a weak driving mechanism. The numerical study was performed in the limit of infinitely weak driving. The model exhibits avalanches starting at the pulled end of the chain. The dynamics of the avalanches and their size and strength distributions are studied in detail. The behavior depends on the value of the damping constant. For moderate values an erratic sequence of avalanches of all sizes occurs. The avalanche distributions are power laws which are a key feature of self-organized criticality. It will be shown that the system selects a state where perturbations are just able to propagate through the whole system. For large damping a regular behavior occurs, where a sequence of states reappears periodically but shifted by an integer multiple of the period of the external potential. There is a broad transition regime between regular and irregular behavior, which is characterized by multistability between regular and irregular behavior. The avalanches are built up by sound waves and shock waves. Shock waves can change their direction of propagation, or they can split into two pulses propagating in opposite directions leading to transient spatiotemporal chaos.

PACS number(s): 05.70.Ln, 05.50.+q, 46.10.+z

I. INTRODUCTION

The Frenkel-Kontorova (FK) model [1] (i.e., a harmonic chain in an external spatially periodic potential) is a favorite model for disordered systems and glassy materials because of its *huge number of metastable states*. The following topics are intensively investigated in the literature: (i) the commensurate-incommensurate transition of the ground state [2], (ii) the lowest excitations in order to calculate the specific heat [3], and (iii) the overdamped dynamics for a strongly tilted external potential in order to understand the pinning-depinning transition of charge-density waves [4].

In 1987 Bak, Tang, and Wiesenfeld [5] showed that in *weakly driven* dissipative systems a huge number of metastable states can lead to a kind of erratic behavior, called *self-organized criticality* (SOC). On the phenomenological level the key feature of SOC is an erratic sequence of events (called *avalanches*) on all scales, i.e., a power-law distribution of the strength of the event. Usually this phenomenon is accompanied by a transient where the distribution does not necessarily show a power law. Finally the system reaches the so-called *SOC attractor*. Bak *et al.* found this behavior in a cellular automaton (dimension ≥ 2) which mimics a sandpile. Later, this and other cellular automata as well as coupled maps were studied in order to investigate SOC [6]. In order to explain the observed power-law distributions Bak *et al.* proposed the following mechanism. The weak driving moves the system to the "edge" of the stability region where it is just critical and therefore exhibits no characteristic scales. The edge represents a threshold for the propagation of a perturbation through the whole system. The crucial point that Bak *et al.* assumed is that a state outside the stability region will stick just at the stability edge during its relaxation towards the stability region. It is interesting to note that in their seminal paper [5] Bak *et al.* used the *overdamped* FK model in order to demonstrate these properties. But they rejected this system for further studies because the same so-called "least-stable" state always reappears, a feature which is shared by their one-dimensional cellular automaton in contrast to the higher dimensional cellular automata that display SOC behavior. Nevertheless, SOC is possible in the FK model if *inertia* is taken into account [7].

The present paper presents results of a detailed study of the weakly driven FK model. The driving mechanism is a slow pulling of the chain at one end. Our study sheds some different light on the complex behavior of the FK model because it is treated in a regime far away from previous investigations: (i) the driving force pushes the system into metastable states with large energies; (ii) this driving mechanism does not decrease the number of meta-stable states as is usually the case in depinning-pinning transition studies; (iii) the dynamics is neither conservative nor overdamped.

To be more specific, a chain of $N+1$ particles, $i = 0, 1, \ldots, N$, of mass $m = 1$ with nearest-neighbor interaction V_I in a spatially periodic external potential V_E is investigated. We assume that all particles are damped with the same damping constant g. The equation of motion is therefore

$$\ddot{x}_i + g\dot{x}_i = V_I'(x_{i-1} - x_i) - V_I'(x_i - x_{i+1}) - V_E'(x_i), \quad i = 1, \ldots, N. \tag{1}$$

Particle $i = 0$ is pulled (or pushed) with constant velocity

$$x_0 = vt \quad \text{with} \quad |v| \ll 1, \tag{2}$$

and particle $i = N$ is the free end of the chain. The latter condition is taken into account by introducing an $(N + 2)$nd variable x_{N+1} chosen in such a way that $V_I'(x_N - x_{N+1}) = 0$. Recently, simulations of the original FK model [7] [i.e., $V_I(x) = (x - a)^2/2$, $V_E(x) = b\cos x$] have been performed, as well as of a FK model with Toda-like nearest-neighbor interaction [8] [i.e., $V_I(x) = e^{-x} + e^{-a}x$, $V_E(x) = b\cos x$] serving as a simplified model of a ferromagnetic Bloch-wall array in a spatially periodic field. In this paper the FK model with a piecewise parabolic external potential (see Fig. 1) is investigated, i.e.,

$$V_I(x) = (x - a)^2/2, \tag{3}$$

$$V_E(x) = b\,(\tfrac{1}{2} - x \bmod 1)^2, \quad b > 0. \tag{4}$$

The general behavior in all cases is the following. The slow pulling (or pushing in the case of the Toda potential) locally puts energy into the system at a very low rate. This drives the system towards an instability at which at least a fraction of this energy is released and propagates along the chain. Since the chain is damped, the energy dissipates and the system settles down in one of the huge number of metastable states. We will call such an event an *avalanche*. It rearranges the configuration of the chain at least locally. Previous studies [7,8] indicate the existence of power laws for the distributions of avalanche strengths measured by taking the sum over all particle displacements during the avalanche. In the overdamped limit the sequence of avalanches becomes regular as expected by Bak *et al.* [5].

The external potential in the FK model can be interpreted as a regular array of pinning centers of equal strength for some objects (e.g., charge-density waves, flux lines, or Bloch walls). SOC-like behavior has also been shown to occur in overdamped models with randomly distributed pinning centers [9,10]. In [9] the same driving mechanism as in our model was used (i.e., pulling the chain at one end). The erratic and SOC-like behavior in those models seems to be caused by the randomness of the external potential. In our case the inertia together with the nonlinear character of the external potential cause irregular avalanches (see Sec. VII) which seem to be responsible for the same type of behavior.

To compare the results with the behavior of cellular automaton models showing SOC it is important to drive

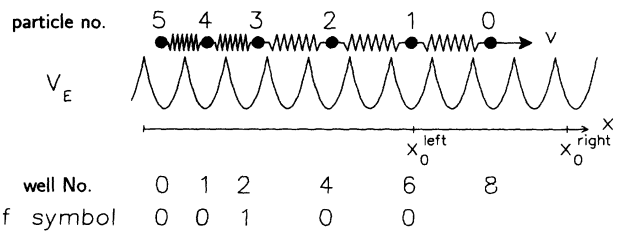

FIG. 1. The Frenkel-Kontorova (FK) model with piecewise parabolic external potential V_E. An example of a stationary state and its well numbers and f symbols are shown. The state is stable for adiabatic moves of the fixed end of the chain (i.e., the zeroth particle) between x_0^{left} and x_0^{right}.

the system very slowly because deviations are expected from finite driving. In other words, a separation of time scales is necessary: a fast time scale is given by the averaged duration of an avalanche, and the slow time scale is defined as the averaged time interval between the occurrence of successive avalanches. Infinitesimally slow driving means that the slow time scale tends to infinity because on average two avalanches are separated by an infinite time interval. The limit of infinitesimally slow driving cannot be reached in computer simulations of continuous systems described by differential equations. Therefore a finite but very small driving is usually chosen to get a compromise between time scale separation and computer time consumption.

The main advantage of a piecewise parabolic external potential is the possibility to do the simulations in the limit of *infinitesimally* slow drive i.e., $v \to 0$. This is due to the fact that all stationary states are uniquely characterized by the integer part n_i of the particle positions x_i which we will call the *well number*. In the next section we show that it is possible to reconstruct the stationary states from the position of the fixed end x_0 and the well numbers. Furthermore, we are able to calculate the stability interval of x_0, i.e., the interval in which an adiabatic move of x_0 does not lead to an avalanche. Therefore, in a computer simulation we abridge the adiabatic move by putting the system into the state at the edge of the next instability.

There is another reason for choosing a piecewise parabolic potential: it is well known from the work of Aubry [2] that in a smooth potential with potential strength below the so-called "analyticity breaking point" the ground state can be shifted without energy because a Goldstone mode exists. Therefore we would expect that no avalanches occur and the chain would creep over the "washboard" V_E. It is also well known that the loss of the Goldstone mode is due to the disappearance of the so-called "last Kolmogorov-Arnold-Moser (KAM) trajectory" in the two-dimensional symplectic map which describes all stationary states. The piecewise parabolic potential leads to a purely hyperbolic map which does not have KAM trajectories.

A model similar to the FK model is the Burridge-Knopoff (BK) model [11], which was proposed as a model of an earthquake fault. In recent years various modifications of it have become popular in order to investigate SOC [12–15]. The main difference from the FK model is that the external potential and damping are replaced by phenomenological stick-slip friction forces. A particle is at rest if the forces resulting from the springs are weaker than the static friction force. Originally the chain is driven by weak springs connecting each particle with a rigid and slowly moving plate. A driving mechanism similar to the one in our model was also studied (train model) [15]. The external potential together with the damping in the FK model can be considered as a microscopic model for a stick-slip friction law. It has the properties [16] that (i) the dynamic friction increases with velocity, and (ii) the static friction is larger than the dynamic friction if the damping constant g is not too large. In that case the friction force is therefore discontinuous

at zero. Avalanches in the BK model are possible only if the dynamic friction is less than the static friction. Otherwise only creeping is possible [17]. Other details (e.g., whether the dynamic friction decreases or increases with velocity) of the various phenomenological friction laws are unimportant.

The paper is organized as follows. Section II deals with stationary states. It gives the tools for solving the problem of infinitesimally slow driving in the simulations. Details of the whole simulation are given in Sec. III. Section IV gives a detailed analysis of the SOC attractor. Section V presents avalanche statistics and attractor dynamics for various values of the model parameters. Section VI presents details of the avalanche dynamics, and also discusses the mechanism which leads to SOC in the FK model. Section VII investigates the transition to the overdamped case. The concluding section compares the results obtained here with results from other models.

II. STATIONARY STATES

This section deals with the stationary states of the FK model with piecewise harmonic external potential. The methods for (i) generating stationary states, (ii) obtaining compact descriptions ("symbolic dynamics") of them, and (iii) calculating points of instability are developed. Furthermore, the number of metastable states is calculated.

The stationary states for a prescribed value of x_0 are given by the solutions of

$$0 = x_{i+1} - 2x_i + x_{i-1} - b[2(x_i \bmod 1) - 1], \quad i = 1, \ldots, N, \tag{5}$$

where x_{N+1} is defined by $x_{N+1} \equiv x_N - a$. It should be noted that every solution of (5) is either stable or metastable, i.e., no linearly unstable solutions exist. This can be shown by calculating the eigenvalues of the matrix given by the second variation of the potential energy. The eigenvalues (i.e., the phonon dispersion relation)

$$\omega_k^2 = 2(1 + b - \cos k) \tag{6}$$

are always positive. Therefore the matrix is positive definite, which proves the stability.

A very general way to solve Eq. (5) is the following (it is also applicable to other FK models [7–9]). Choose an arbitrary value of x_N and then calculate iteratively the sequence $x_{N-1}, x_{N-2}, \ldots, x_1, x_0$. Change x_N slightly until x_0 matches its prescribed value. This is not an effective way to calculate *all* stationary states but it shows that *each* stationary state is *uniquely* determined by x_N. Furthermore, we can think of x_0 as a function of x_N. For $N \to \infty$ this function will be nowhere differentiable and the cut of it with a horizontal line gives a Cantor-like set. Every point in this set corresponds to a certain stationary state.

In our case $x_0(x_N)$ is piecewise linear since the external potential is piecewise harmonic. The pieces are produced by the modulo term $x_i \bmod 1$ of Eq. (5) at each step of the iterative computation of this function. They all have the slope $(1 + 2b)^N$ and they are separated by jumps of height $2b$ (see Fig. 2) [18]. The lower and upper values of each piece determine the interval inside which x_0 can vary slowly without releasing an avalanche. At the boundary of that interval some particle is exactly on a cusp of the external potential. This particle will be destabilized if x_0 is moved slightly beyond the boundary. The important point is that we are able to calculate this stability interval for a given stationary state.

The key for an effective method to generate all stationary states for a prescribed x_0 is the existence of a compact description, called "symbolic dynamics," for all stationary states. Each description is a list of exactly N symbols which determines *uniquely* a stationary state. We present two of them.

In the first symbolic dynamics the symbols, called *well numbers* (see Fig. 1), are the integer parts $n_i \equiv \mathrm{Int}(x_i)$ of the positions x_i [19]. By applying the Green's function method on $2(b + 1)x_i - x_{i+1} - x_{i-1} = b(1 + 2n_i)$ it is easy to show that the positions x_i can be reconstructed uniquely by x_0 and the well numbers n_i:

$$x_i = C \sum_{j=1}^{N} (1 + 2n_j)\eta^{|i-j|} + \alpha_0 \eta^i + \alpha_N \eta^{N-i}, \tag{7}$$

with

$$C = \frac{b/2}{\sqrt{b(b+2)}}, \tag{8}$$

$$\eta = 1 + b - \sqrt{b(b+2)}. \tag{9}$$

The coefficients α_0 and α_N are given by the solutions of

$$\alpha_0 + \eta^N \alpha_N = x_0 - C \sum_{i=1}^{N} (1 + 2n_i)\eta^i, \tag{10a}$$

$$-\eta^N \alpha_0 + \eta^{-1} \alpha_N = -\frac{a}{1 - \eta} + C \sum_{i=1}^{N} (1 + 2n_i)\eta^{N-i}. \tag{10b}$$

Clearly Eq. (7) does not hold for arbitrary well numbers.

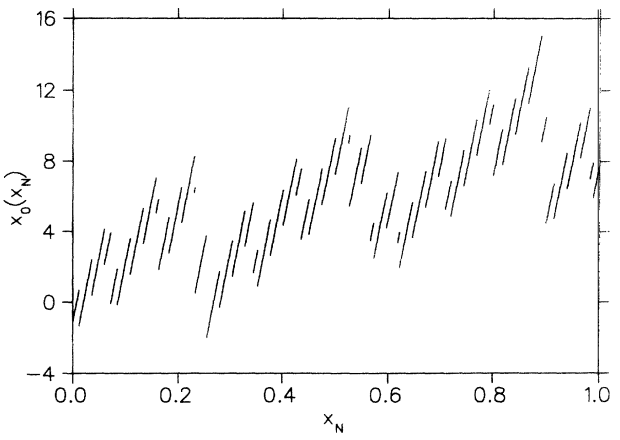

FIG. 2. The fixed end of the chain x_0 as a function the free end x_N. The parameters are $a = 1.3$, $b = 1$, and $N = 4$.

Only such well number configurations are allowed which fulfill the self-consistency condition

$$n_i = \mathrm{Int}(x_i), \quad i = 1, \ldots, N, \tag{11}$$

where Int means integer part of. If a stationary state is given we obtain a compact description of it by calculating the well numbers. Using (7) we can completely reconstruct the stationary state from the well numbers, i.e., there is a one-to-one relation between $\{x_1, \ldots, x_N\}$ and $\{n_1, \ldots, n_N\}$.

There is an even more compact description by using the so-called *f symbols* (see Fig. 1) defined by

$$f_i = n_{i+1} - 2n_i + n_{i-1}, \quad i = 1, \ldots, N, \tag{12}$$

with $n_{N+1} \equiv n_N - \mathrm{Int}(a)$ and $n_0 = \mathrm{Int}(x_0)$. The f symbols give a rough estimate of the resultant force on the particles due to the springs (i.e., $x_{i-1} - 2x_i + x_{i+1}$ which should be less than b). Using (5) we obtain the following inequality:

$$|f_i| \leq \mathrm{Int}(2 + b). \tag{13}$$

For given f symbols we get for the well numbers

$$n_i = \mathrm{Int}(x_0) - i\,\mathrm{Int}(a) - \sum_{j=1}^{N} \min(i, j)\, f_j. \tag{14}$$

For particles in the bulk of the chain the position relative to the potential well can be calculated directly from the f symbols:

$$x_i \bmod 1 = x_i - n_i = \frac{1}{2} + \frac{C}{b} \sum_j f_{i+j} \eta^{|j|}. \tag{15}$$

This formula is obtained from Eqs. (7) and (14) by shifting the limits of the sums to $\pm\infty$ and by dropping the α terms in (7).

Next we describe a method for generating an arbitrary stationary state. As a by-product we also get the stability interval. The method simply iterates intervals by using Eq. (5). We start with the interval $[0, 1)$ assuming well number zero for the Nth particle. One iteration step leads to the interval $[-a - b, 1 - a + b)$ which gives the possible positions of particle number $N - 1$. In the next iteration the modulo term in Eq. (5) cuts this interval into subintervals since its length is greater than unity. Because each subinterval should be treated separately we have to choose which interval we want to iterate further. The subintervals are uniquely labeled by the well number because the cuts occur at integer points. This iteration scheme leads immediately to the stability interval $(x_0^{left}, x_0^{right})$ because after we have chosen the well number of particle $i = 1$ we get the interval of all possible positions of particle $i = 0$ (i.e., the fixed particle) after the next iteration step.

We finish this section with the calculation of the numbers of metastable states. With the method of the last paragraph the total number of metastable states $M(N)$ can easily be calculated numerically. For large N this number increases exponentially with N. The rate of increase is the *topological entropy* ν, i.e.,

$$\nu = \lim_{N \to \infty} \frac{\ln M(N)}{N}. \tag{16}$$

We can calculate ν *analytically* with the following considerations. First we rewrite Eq. (5) in the form

$$\begin{aligned} d_{i+1} &= d_i + b[2(x_i \bmod 1) - 1], \\ x_{i+1} &= x_i + d_{i+1}. \end{aligned} \tag{17}$$

This is a two-dimensional symplectic map similar to Arnold's cat map [20] ($b = 1/2$ corresponds to the original cat map). Next we use a theorem of Pesin which says that the metric (or Kolmogorov-Sinai) entropy is given by the sum of the positive Lyapunov exponents averaged over the invariant density [20]. The Lyapunov exponents of the map (17) are $\pm \ln \eta$. Because the invariant density of the map (17) is constant [20] the topological entropy is equal to the metric entropy; therefore we get

$$\nu = -\ln \eta = \ln[1 + b + \sqrt{b(b+2)}]. \tag{18}$$

This result is verified by direct numerical calculations.

III. NOTES ABOUT THE SIMULATION

In order to simulate infinitesimally slow driving (i.e., pulling speed $v \to 0$) the simulation scheme is broken up into two steps which are repeated as often as desired.

Driving step. For a given stationary state first the well numbers n_i and the stability interval $(x_0^{left}, x_0^{right})$ of the position of the fixed end of the chain x_0 are calculated according to Sec. II. Then x_0 is put near the edge but still within the stability interval, i.e., $x_0 = x_0^{right} - \epsilon$, where $\epsilon \ll 1$. Without changing the well numbers the new positions x_i are calculated according to Sec. II. Only the positions of the particle near the fixed end are noticeably shifted because the change is proportional to η^i. Finally, x_0 is put just outside the stability interval, i.e., $x_0 = x_0^{right} + \epsilon$. In all simulations we have chosen $\epsilon = 10^{-4}$.

Relaxing step. For the simulation of the avalanche dynamics we use a predictor-corrector scheme described in Ref. [21] which is superior to the well-known Verlet algorithm [22] especially for potentials with cusplike singularities [21]. For the time step Δt of the integration scheme we have chosen 0.01, 0.005, and 0.001 for $b = 1$, $b = 5$, and $b = 20$, respectively. These time steps are smaller at least by a factor of 200 than the fastest oscillation periods given by the maximum of the phonon dispersion relation (6).

Because of dissipation of energy the avalanche dies out. We use the following criterion for the death of an avalanche. The barrier for a flip of a single particle into a neighboring potential well is calculated under the assumption that the neighboring particles are fixed. Because this barrier height is only approximately correct we require that the kinetic energy should be less than one tenth of this barrier height. If this criterion is fulfilled for all particles the simulation for a single avalanche is stopped.

There is a strong similarity to cellular automata showing SOC [6] where also a distinction is made between driving rules and relaxing rules which are applied to stable states and unstable states, respectively. These automata can be seen to be driven in an "infinitely slow" limit because the driving rules are not applied before even the largest avalanche has died out.

We end this section with some remarks about the values we have chosen for the four system parameters a, b, N, and g. In the study of the ground state of the FK model the ratio between equilibrium length of the springs and potential periodicity plays an important role [2]. In our case this ratio is unimportant, because the chain is driven far away from the ground state (see next section). Only the strength and the probability of the smallest avalanches are slightly changed. In fact most of the energy is stored in the springs. We have chosen the following values: equilibrium length $a = 1.3$; strength of the external potential $b = 1$, 5, and 20; number of particles $N = 125$ and 500 usually; damping constant $g = 10^{-3}$–10. If not mentioned otherwise, all results are obtained from simulation runs of 2×10^4 avalanches except for $b = 20$ where the number of avalanches was only 10^4.

IV. THE SOC ATTRACTOR

The separation of time scales caused by the infinitesimally slow driving leads to the definition of *two* phase spaces. The first one is the usual phase space of a mechanical system defined by the positions and momenta of all particles (including the zeroth particle). The second phase space, called *reduced phase space*, a subspace of the former one, is defined by all stationary states modulo an integer amount of the potential periodicity. A point of it is given by the f symbols of the stationary state. From Sec. II we know that the particle positions can be reconstructed from the f symbols except that of particle number zero (the fixed end). This is not a restriction because only the stability interval $(x_0^{left}, x_0^{right})$ is needed, which can be calculated from the f symbols. The reduced phase space is discrete and finite, similar to the phase space of cellular automata showing SOC [6]. Unstable states of these automata correspond to unstable states of the reduced phase space (i.e., sequences of f symbols which do not correspond to stationary states of the chain). The dynamics of an avalanche takes place in the full phase space and cannot be uniquely projected onto the reduced phase space.

Similarly to the distinction between two phase spaces, we distinguish between the usual *physical time* t and an integer *pseudotime* τ which will be increased by unity after each occurrence of an avalanche. We also distinguish between the *full dynamics* taking place in the full phase space and the *reduced dynamics* which is a discrete dynamics on the reduced phase space. The reduced phase space is defined in such a way that an avalanche shifting the chain by one period of the potential leads to an orbit of period 1. The reduced dynamics can be interpreted as a cellular automaton with complicated nonlocal rules. From the simulation scheme described in Sec. III we see that the automaton is completely deterministic. The automaton would be a stochastic one if we took into account the unavoidable thermal noise which will be amplified by the chaotic nature of the avalanche dynamics (see Sec. VI).

The physical time t is not useful to describe the whole dynamics since the mean time between successive avalanches goes to infinity for pulling velocity $v \to 0$. Instead, we use $x_0 = vt$. Remember that during a single avalanche x_0 is constant. In Sec. V we will see that, on average, $x_0(\tau + 1) - x_0(\tau)$ remains finite even for $v \to 0$. Presumably, it will be independent of v for at least very small values. Thus, knowing the distribution of $x_0(\tau + 1) - x_0(\tau)$, we are able to calculate the distribution of waiting times between successive avalanches.

Starting with the ground state the driving mechanism will stretch the chain. Most of the avalanches release less energy than the work due to stretching which is put into the system between successive avalanches. This is still true after a transition time where the system reaches an attractor in the reduced phase space (see Fig. 3). The transition time usually ends after the occurrence of the first avalanche involving all particles of the chain.

We call this attractor the *SOC attractor* though the avalanche distribution may strongly deviate from an expected power-law behavior (see Sec. V). It is a *self-organized* balance between driving, which puts energy into the system, and avalanching, which dissipates energy. The motion on the SOC attractor looks erratic although we know that it can only be a periodic orbit because of the finiteness of the reduced phase space. But the recurrence time is very large, presumably of the same

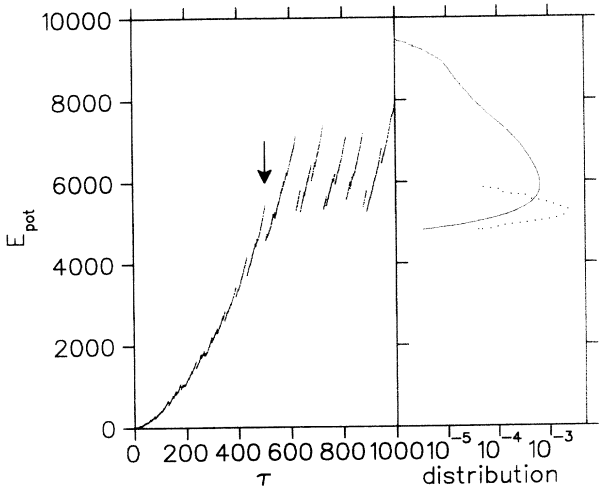

FIG. 3. Transient and SOC attractor of the reduced dynamics. The parameters are $b = 1$, $N = 125$, and $g = 0.1$. The initial state is defined by $f_i = 0$ for $i = 1, \ldots, N$. The first avalanche which involves the whole chain is marked by an arrow. The energy distributions of the SOC attractor and of 5500 relaxation experiments with $\overline{f} = 0.6$ (for details, see text) are denoted by a solid line and a dotted line, respectively.

order as the number of stationary states. Thus it increases exponentially with the number of particles.

In order to characterize the SOC attractor we first discuss the distribution of the potential energy

$$E_{pot} \equiv \sum_{i=1}^{N} V_I(x_{i-1} - x_i) + V_E(x_i). \tag{19}$$

The potential energy is calculated at the instability point $x_0 = x_0^{right}$ just before the avalanche starts. The simulations show that the mean potential energy $\overline{E}_{pot}$ clearly scales with N^3. This scaling behavior can be easily understood if we assume that, on average, the *local stress* of the chain $x_{i-1}+x_{i+1}-2x_i$ is the same for each particle in the bulk of the chain. Therefore the length of the springs decreases linearly with the particle index from strongly stretched at the fixed end to almost equilibrium length at the free end. Using $\sum_{i=1}^{N} i^2 = N(N+1)(2N+1)/6$ we get

$$\overline{E}_{pot}/N^3 = \frac{\overline{f}^2}{6} + O(N^{-1}), \tag{20}$$

where $\overline{f} \equiv \overline{x_{i-1} + x_{i+1} - 2x_i}$ is the mean local stress which is equivalent to the mean f symbol per particle. Using Eq. (5) it can be expressed in terms of the mean position of the particle related to the potential well:

$$\overline{f} = b\,(2\,\overline{x_i \bmod 1} - 1). \tag{21}$$

Figure 4 shows that $\overline{x_i \bmod 1}$ (and therefore also $\overline{f}$) is independent of i. The deviation between $\overline{f}$ calculated from Eq. (20) and from Eq. (21) is less than 1%. Since the states are analyzed at the stability boundary x_0^{right} the value 1 for $\overline{x_i \bmod 1}$ at $i = 1$ expresses the fact that almost all avalanches start at the first particle.

The mean SOC attractor is similar to the attractor obtained by pulling the chain with finite velocity v through a viscous medium with no external potential (i.e., $b = 0$). Here all particles travel with v. From the equation of motion (1) we get $x_{i-1}+x_{i+1}-2x_i = gv$. Thus the potential energy scales also like N^3.

Figure 5 shows $\overline{E}_{pot}/N^3$ for several values of b and g. The mean potential energy increases with b and g. The increase with b does not originate from the increase of energy stored in the external potential, but from the fact that the stretching of the springs can be increased because of stronger particle pinning. The approximate power law in g (exponent ≈ 1.5) is similar to the power-law behavior of residual energy as a function of cooling rate expected in glassy materials [23]. This expectation was recently confirmed [24] by simulations of a mechanical model similar to the FK model (a chain of particles with anharmonic on-site potential and harmonic nearest-neighbor interactions). The cooling was simulated by viscous damping (cooling rate proportional to damping constant); the energy of the initial state was large enough to allow the system to move in phase space *unhindered* by potential barriers. Similar annealing simulations with the FK model lead to residual energies much below the mean energy of the SOC attractor because the residual energy scales only with N. On the other hand, simulations starting with *stable* initial states with potential energies much larger than the mean energy of the SOC attractor show that, on average, the energy of the state after the first avalanche is almost identical with the mean energy of the SOC attractor (see dotted energy distributions in Fig. 3) as expected for SOC [6].

The distribution of the potential energy of the SOC attractor is strongly non-Gaussian. Figure 3 (solid line) shows a typical example: a steep Gaussian-like increase, a pronounced maximum, and a slow exponential-like decrease. There seems to be no universal distribution function which can be rescaled for different values of N, b, and g in order to fit the data. Therefore no scaling laws for the width of the distribution are expected. We only found that the increase is stronger than N^2 but weaker than N^3. Hence the relative width decreases with N.

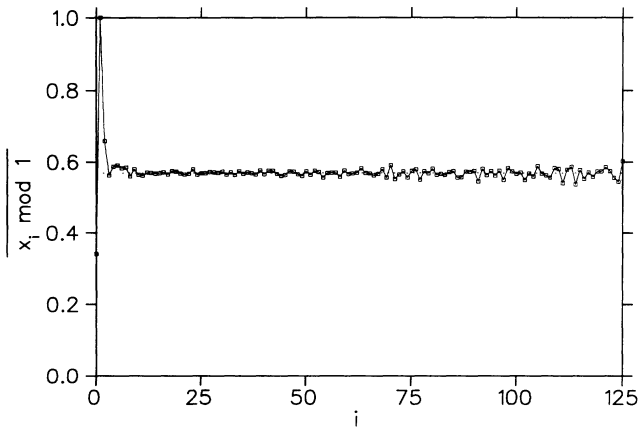

FIG. 4. Temporal average of $x_i \bmod 1$ over 15 000 avalanches. The parameters are $b = 1$, $N = 125$, and $g = 0.1$. The dotted line is the expected value assuming no i dependence and using Eqs. (20) and (21).

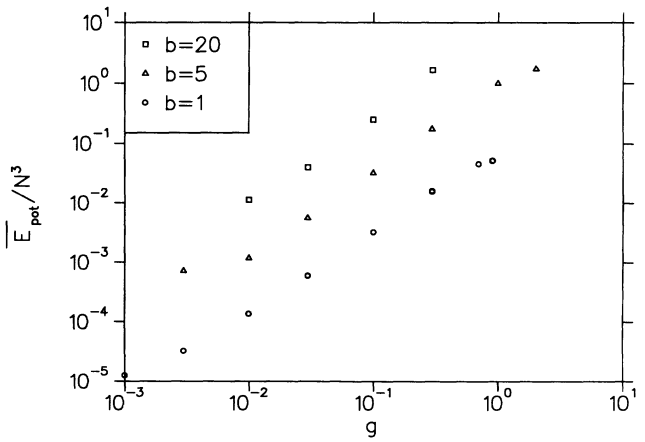

FIG. 5. The mean potential energy $\overline{E}_{pot}$ as a function of the damping constant g. The results are obtained from simulations with $N = 500$ and $N = 125$ for $b \leq 5$ and $b = 20$, respectively.

The dotted line in Fig. 3 shows the energy distribution of the states into which stable states having very large energies relax after the first avalanche. The distribution is a sharp peak at the position near the steep Gaussian-like increase of the distribution of the energy of the SOC attractor. This fact is consistent with the observation that very large avalanches of states of the attractor with energies large above the mean value leave the system in a state almost at the place of the sharp peak (see Fig. 3).

A typical distribution of $x_i \bmod 1$ is shown in Fig. 6. An enlargement shows the self-similar character of this distribution. If we were to generate stationary states by iterating the map (17), all positions would be equally probable because the invariant density is uniform (see Sec. II). The driving mechanism selects states with a potential energy from a relatively small subinterval. Thus the selecting mechanism forbids certain symbols or symbol sequences. For example, for $b = 1$ and $g = 0.1$ the f symbols ± 2 become almost forbidden symbols [the probabilities are $p(-2) = 2.1 \times 10^{-4}$ and $p(2) = 4.7 \times 10^{-3}$] whereas in the case of no selection $p(\pm 2) = 1/8$. The loss of symbols is reflected by the loss of possible values for $x_i \bmod 1$ because of (15). The fractality of the distribution is a well-known consequence of this fact (note, e.g., the classical construction of the Cantor set, where

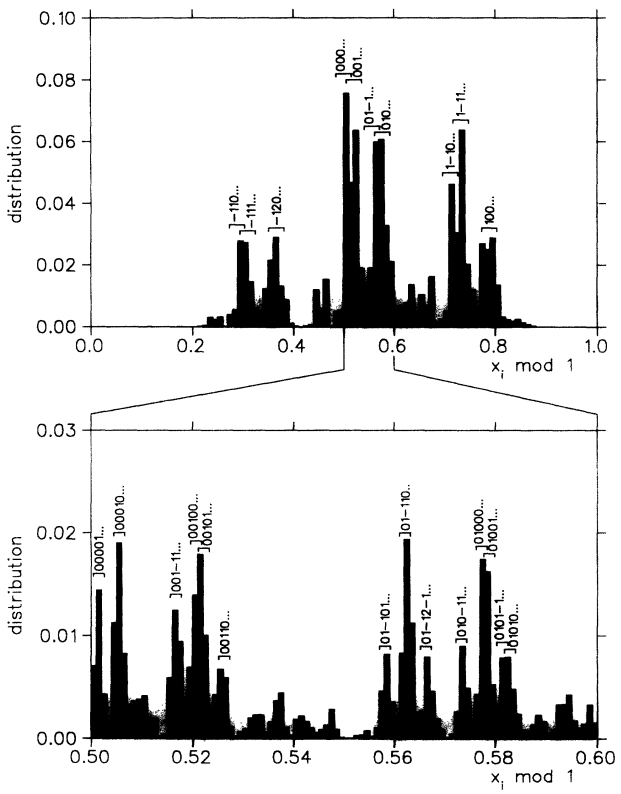

FIG. 6. Distribution of $x_i \bmod 1$ averaged over the bulk particles (i.e., from $i = 10$ until $i = 115$). Parameters are $b = 1$, $N = 125$, and $g = 0.1$. The larger peaks are marked by sequences of sums of f symbols. A sequence is defined by $f_i, f_{i-1} + f_{i+1}, f_{i-2} + f_{i+2}, \cdots$. The square bracket denotes the width of possible values assuming $f_j \in \{-1, 0, 1\}$.

one of three symbols is forbidden). Note that $x_i \bmod 1$ is not uniquely given by the f-symbol sequence; we need $x_i \bmod 1$ and $x_{i+1} \bmod 1$ in order to get the f-symbol sequence. Thus Fig. 6 is in fact a projection of a two-dimensional fractal distribution.

V. AVALANCHE STATISTICS AND THE DYNAMICS ON THE SOC ATTRACTOR

After presenting the statistical properties of the SOC attractor we investigate the reduced dynamics on it. First, we are looking at the distribution of avalanches.

There are several properties of an avalanche which can be measured:

Strength. There are two ways to measure the strength of an avalanche:

(a) The most natural way is to measure the difference ΔE_{pot} of the potential energies just before and after the avalanche. Note again that for most avalanches (i.e., for all small avalanches) ΔE_{pot} is less than the energy put into the system between two successive avalanches (see Fig. 3).

(b) Another way usually used in connection with the BK model is to sum over the displacements of all particles before and after the avalanche,

$$S = \sum_{i=1}^{N} |x_i^{after} - x_i^{before}|. \tag{22}$$

If $x_i^{after} > x_i^{before}$ holds for all i then S/N is equivalent to the displacement of the center of mass.

Length. Almost all avalanches start at the first particle (only for large values of g is there a considerable number of avalanches starting at the second or third particle). Therefore we can define the length L of an avalanche as the index of the furthest particle changing its well number:

$$L = \max\{i \in \{1, \ldots, N\} | n_i^{after} \neq n_i^{before}\}. \tag{23}$$

Duration. As the duration D of an avalanche we define the time needed to fulfill the stopping criterion (see Sec. III).

In the following we present cumulative densities of all these properties. The cumulative density $p(x)$ is the probability p to find an event y greater than x. If it is a power law of the form $p(x) \propto x^{-B}$ the event distribution is also a power law, i.e., $\rho(x) \equiv dp/dx \propto x^{-B-1}$.

Figures 7(a)–7(c) show cumulative densities of avalanche strength for $b = 1$, $b = 5$, and $b = 20$, respectively. All curves are shifted by $\log_{10} g$. We do not find pure power laws. There are of course finite-size cutoffs for very strong avalanches and steps for very weak avalanches caused by the discreteness of the reduced dynamics. But the intermediate parts do not show nice straight lines. For low damping values we see a pronounced crossover on Figs. 7(a) and 7(b). Above the crossover (i.e., for strong avalanches) a power law emerges which becomes visible only if the number of particles N is large enough.

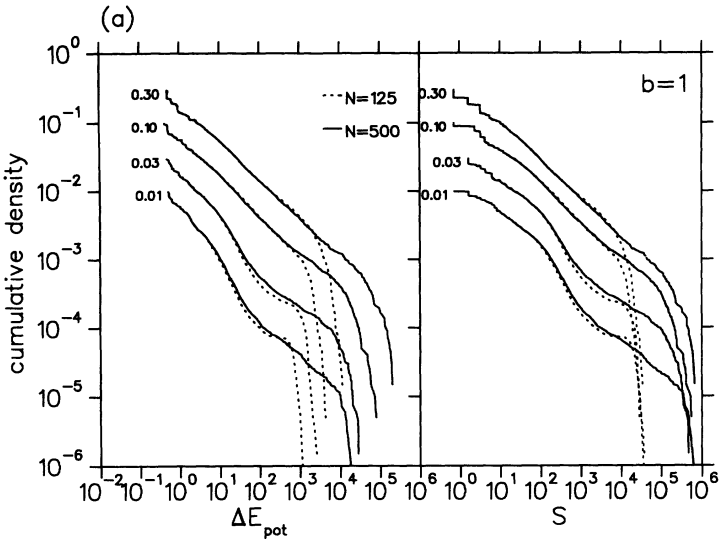

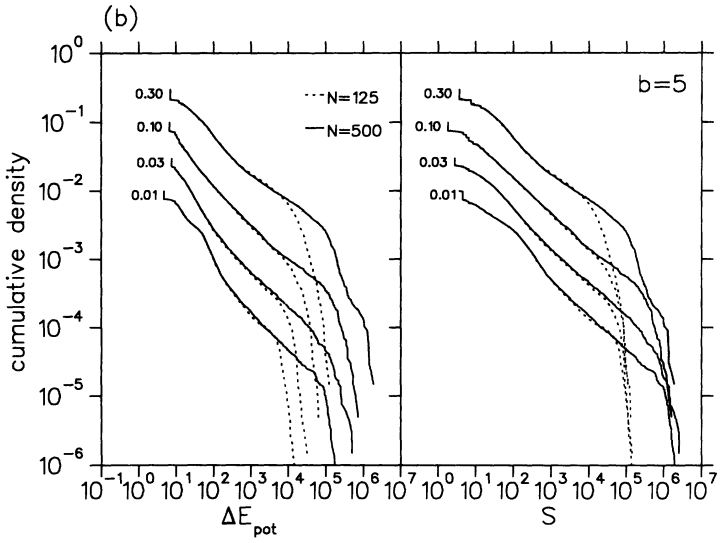

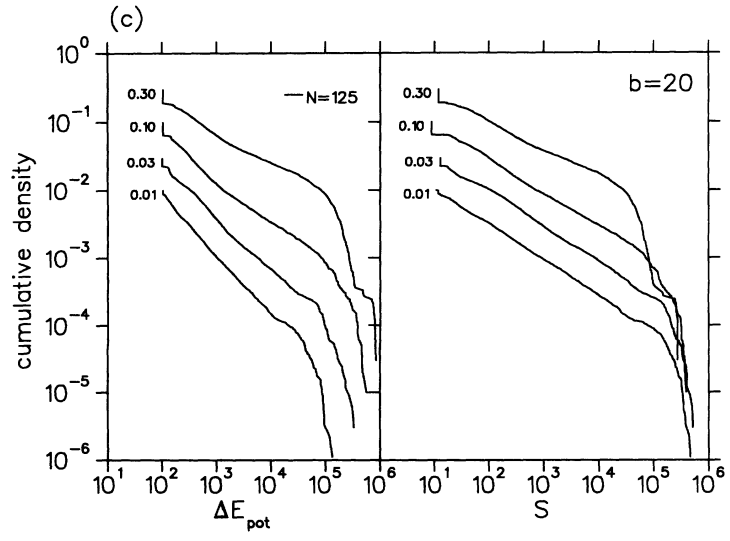

FIG. 7. Cumulative densities of avalanche strengths. The curves are denoted by g and they are shifted by $\log_{10} g$.

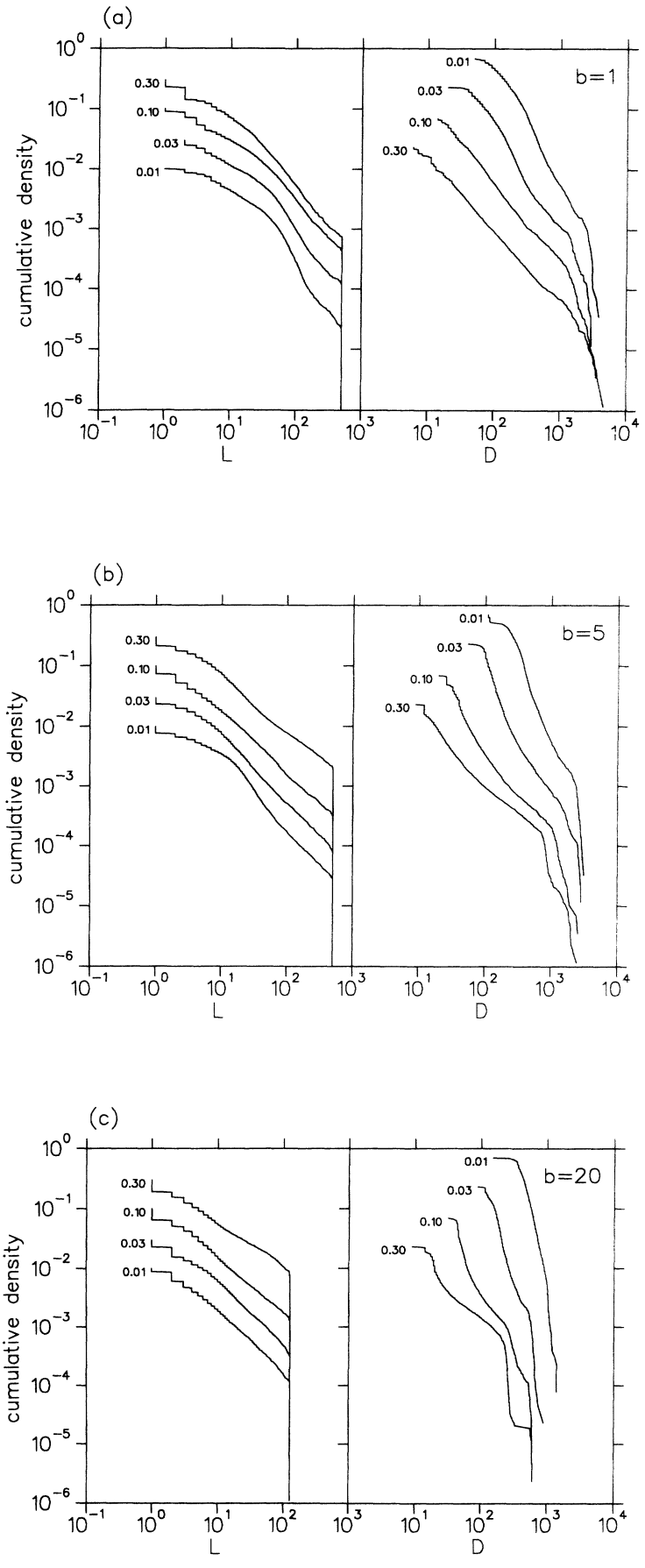

FIG. 8. Cumulative densities of avalanche lengths and durations for (a,b) $N = 500$ and (c) $N = 125$. The curves are denoted by g and they are shifted by $\log_{10} g$.

In Fig. 7(a), for example, it is not seen for $N = 125$ because N is too small. Presumably the power law found for $N = 500$ continues for larger N and the finite-size cutoff shifts to higher values. This is confirmed by a simulation with 2000 particles for $b = 1$ and $g = 0.3$. The exponents $B^{(\Delta E_{pot})}$ and $B^{(S)}$ vary between 0.4 and 0.6. Similar values are found for the FK models treated in [7,8]. For large values of b and small damping values $B^{(\Delta E_{pot})}$ becomes larger than $B^{(S)}$. An example is shown in Fig. 7(c) for $b = 20$ and $g = 0.01$. Here $B^{(\Delta E_{pot})} \approx 0.8$ and $B^{(S)} \approx 0.5$.

Figures 8(a)–8(c) show cumulative densities of avalanche length and duration. Distributions of length are qualitatively similar to distributions of strength. There is also a crossover for $b \leq 5$ and small damping. The crossover shifts to lower values of L if b increases. Above the crossover (i.e., for large avalanches) the power-law exponent $B^{(L)}$ is roughly equal to unity. The significant drop at $L = N$ means that the probability of an avalanche affecting the whole chain $p(L = N)$ is much larger (usually by two orders of magnitude) than the probability for the largest avalanche which just stops before the end. The absolute value of $p(L = N)$ varies between 2×10^{-3} and 2×10^{-2}. Distributions of duration show power laws only for $b = 1$, $g = 0.1$, and $g = 0.3$ with $B^{(D)} \approx 1.5$ and $B^{(D)} \approx 1.3$, respectively.

In order to study the dynamics on the attractor it would be useful to have some visualization of the trajectories on it. One way is to print a list of f-symbol sequences representing successive states. But it would be difficult to interpret this list. For example, a jump of one particle into its neighboring potential well leads to a change not only of its own f symbol but also of the f symbol of its neighbors. Therefore we choose a different representation. From Sec. IV we know that the position of each particle is roughly given by $x_i \approx x_0 - a\,i + i(i - 2N - 1)\overline{f}/2$. If this relation is exact, $x_i + a\,i + i(2N + 1 - i)\overline{f}/2$ plotted as a function of i would give straight lines. Figure 9 shows what actually happens: we get wiggly lines instead of straight lines. Since an avalanche usually involves only the part of the chain near its fixed end, these lines build up a treelike structure. The height of a branching point is the length L of the avalanche whereas the area between two lines is

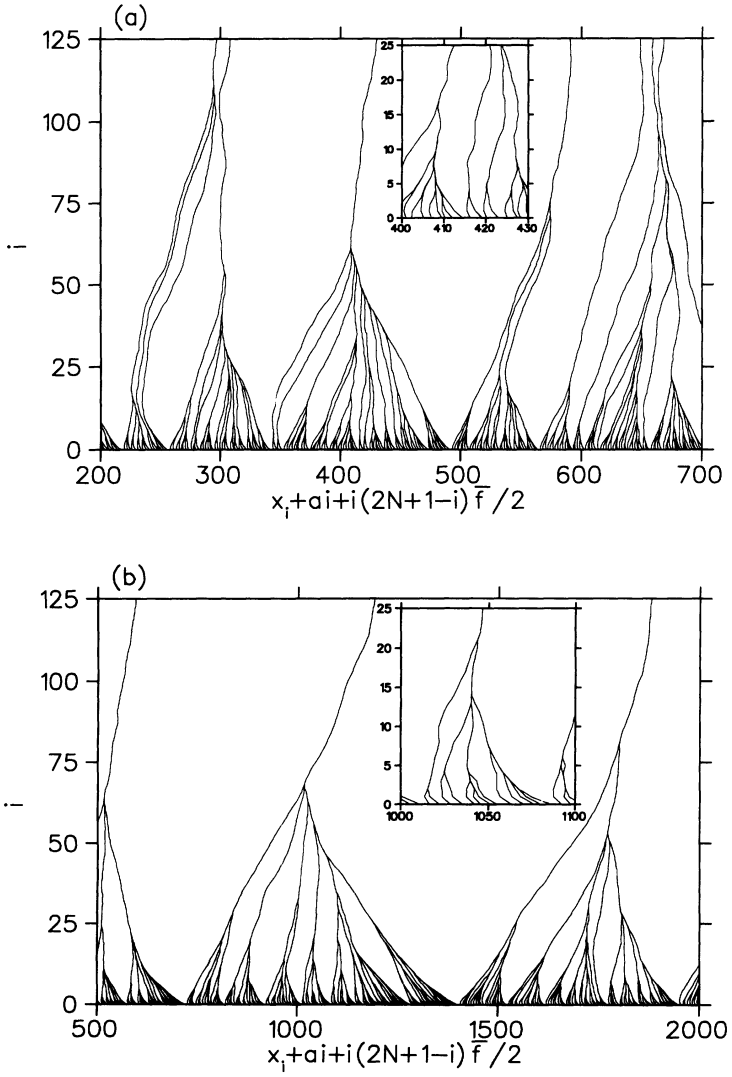

FIG. 9. Examples of trajectories on the SOC attractor for (a) $b = 1$, $N = 125$, and $g = 0.1$ and (b) $b = 5$, $N = 125$, and $g = 0.03$. The states just before an avalanche are drawn. The mean shape of the chain $i(i - 2N - 1)\overline{f}/2 - a\,i$ is subtracted from x_i, where (a) $\overline{f} = 0.138$ and (b) $\overline{f} = 0.187$.

the strength S. An inspection of the figures shows that almost always $x_i(\tau+1) > x_i(\tau)$. Therefore S/N is the displacement of the center of mass.

From Fig. 9 we also see that, on average, x_0 has to be shifted by a finite amount in order to trigger the next avalanche. Because of (2) x_0 is proportional to the time. Therefore $x_0(\tau+1) - x_0(\tau)$ is the waiting time between successive avalanches measured in time units given by the inverse pulling speed v. Figure 10 shows distributions of $x_0(\tau+1) - x_0(\tau)$. They are also self-similar like the distributions of $x_i \bmod 1$ (see Fig. 6). From Sec. II we know that $x_0(\tau+1) - x_0(\tau) < x_0^{right} - x_0^{left} = 1/\eta$. Choosing stationary states randomly, x_0 would be equally distributed between x_0^{left} and x_0^{right}. Therefore we expect the mean value $\overline{x_0(\tau+1) - x_0(\tau)} = \eta^{-1}/2$. From the simulation where a specific selection takes place we found that the mean value is always less than $\eta^{-1}/2$. It increases with decreasing damping and seems to approach this value for $g \to 0$.

One might expect that a tiny shift of x_0 may trigger an avalanche. But this not the case (see Fig. 10). There is a gap near zero where the probability to find a value for $x_0(\tau+1) - x_0(\tau)$ in this gap is almost zero. Although the system is driven far away from equilibrium and a huge amount of energy is stored in the chain, a *finite* amount of energy is needed in order to trigger an avalanche. For large values of the damping constant the gap shrinks to zero and a finite density at zero appears. As a consequence we also find avalanches which start not at the first particle but at particles deeper in the chain.

From experiments on two objects which are in dry contact and which are moved very slowly against each other it is well known that the pulling force fluctuates. It is expected that the power spectra of these fluctuations will show a power law $1/f^{B^{(F)}}$ [25,26]. Figure 11 shows the pulling force as a function of x_0. The pulling force is $x_0 - x_1 - a$. The jumps correspond to avalanches. The power law clearly shows $1/f$ noise. For weaker damping the exponent $B^{(F)}$ increases and seems to reach 2 for $g \to 0$. The oscillations in the power spectra are caused by the nearly periodic appearance of the avalanches. Therefore the frequency of the first peak is roughly given

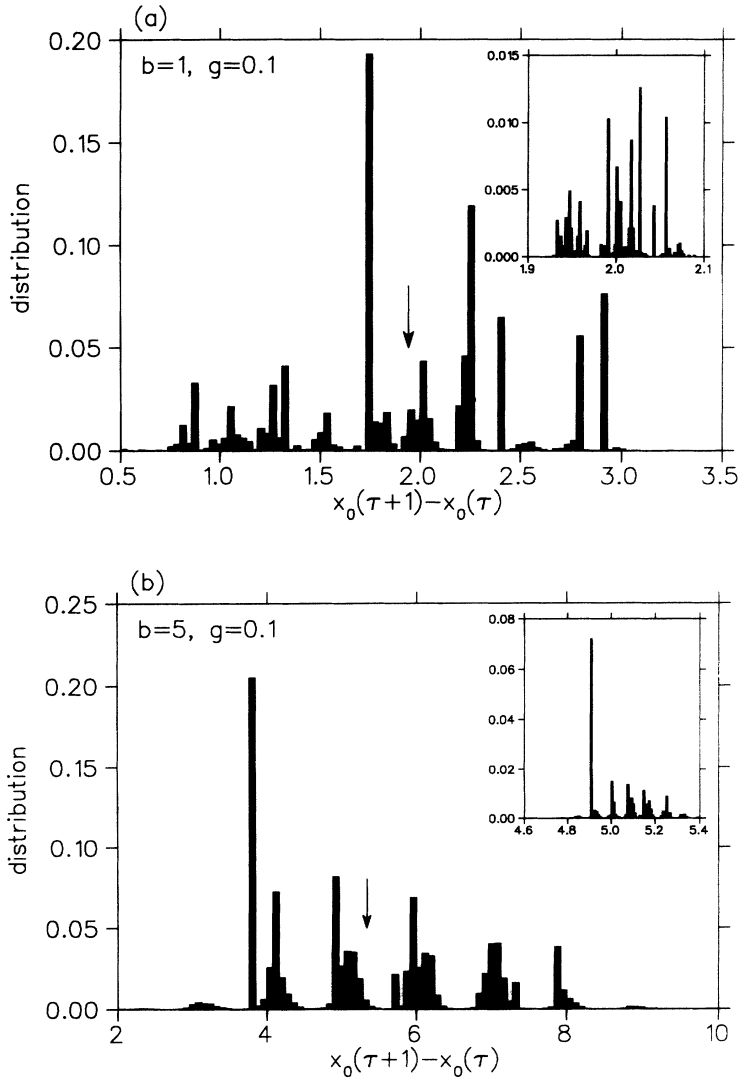

FIG. 10. Distribution of $x_0(\tau+1) - x_0(\tau)$ for (a) $b = 1$, $N = 250$, and $g = 0.1$ and (b) $b = 5$, $N = 125$, and $g = 0.1$. It is also the distribution of the waiting time between successive avalanches in accordance with Eq. (2). The arrow denotes the mean value.

by $1/\overline{x_0(\tau+1)-x_0(\tau)}$. These results are independent of the chain length N and nearly independent of the potential strength b.

VI. DETAILS OF SINGLE AVALANCHE DYNAMICS

In this section we take a closer look at the dynamical process of a single avalanche. This will give us some insight into the question of how the chain is able to organize itself into a critical state.

Figures 12 and 13 show for $b = 1$ and $b = 5$, respectively, two typical examples of large avalanches which do not hit the end of the chain. The dynamics are visualized by (a) kinetic energy plots where a gray scale shows the kinetic energy of each particle averaged over a time period given by the smallest phonon frequency, and (b) displacement plots where for equidistant time steps the displacement of each particle from its initial value is drawn. We easily see two types of propagations.

Sound waves. These are the smooth waves at low level in the kinetic energy plots. They are *linear* waves. From the phonon dispersion relation (6) we immediately calculate the sound velocity v_S as

$$v_S = \max_k \frac{d\omega_k}{dk} = \eta^{1/2}, \tag{24}$$

where η is given by (9). This formula agrees very well with the sound waves found in the simulations.

Shock waves. These are the sharp waves at high level in the kinetic energy plots. They are *nonlinear* waves of propagating hopping events. This is easily seen in the displacement plot of the first shock wave which starts at the first particle and propagates to the right. Shock waves can stop at certain points. They can be partially or totally reflected at some points. Thus they propagate in different directions and most particles will be hit by more than one shock wave. A shock wave is often accompanied by several delayed shock waves propagating in the same direction. The velocity is not constant during a shock wave but varies only slightly. However, it is always larger than the sound velocity. The driving mechanism is the release of energy during particle hopping. We give a rough estimate of the released energy E_{rel} of a single par-

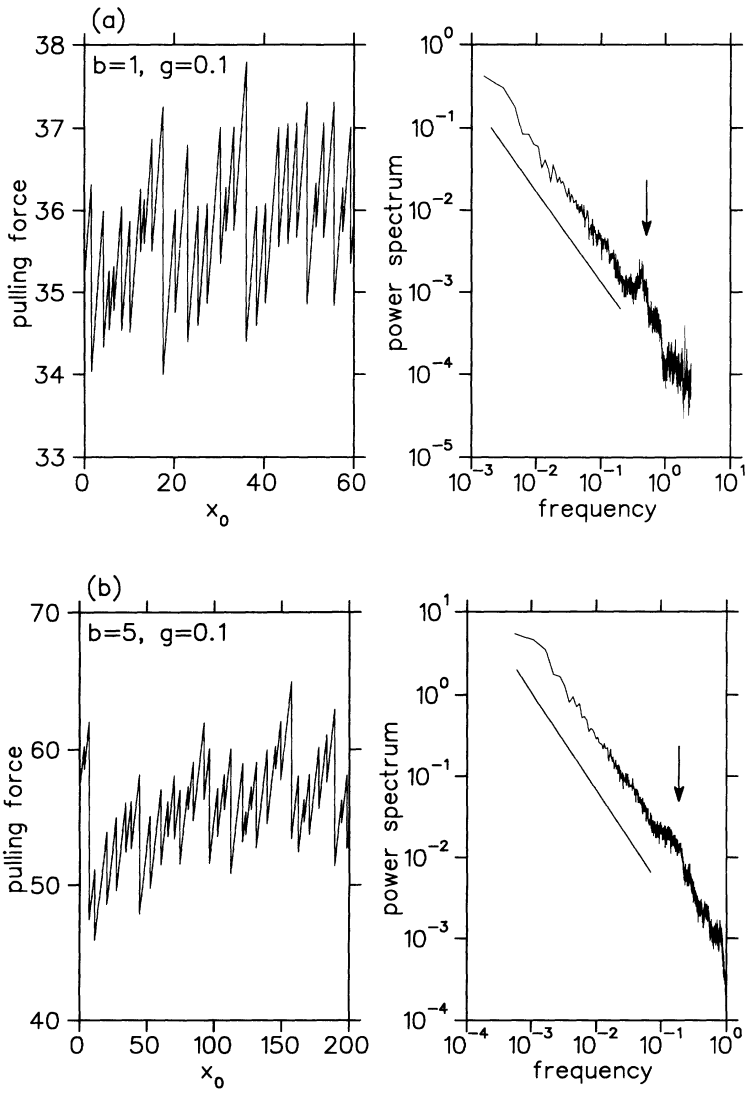

FIG. 11. Pulling force and its power spectrum for (a) $b = 1$, $N = 250$, and $g = 0.1$ and (b) $b = 5$, $N = 125$, and $g = 0.1$. The line has the slope -1.1 and -1.2 for (a) and (b), respectively. The arrows denote the frequencies corresponding to the mean distance between two successive jumps of the pulling force.

ticle hopping. Compare two configurations where only one particle changes its position from x_i^{before} to x_i^{after}. Neglecting the energy of the external potential we get $E_{rel} = (x_i^{after} - x_i^{before})(x_{i+1} + x_{i-1} - x_i^{after} - x_i^{before})$. On average, we get

$$E_{rel} \approx \bar{d}\,\bar{f}, \tag{25}$$

where $\bar{d}$ is the averaged displacement $x_i^{after} - x_i^{before}$ and $\bar{f}$ is the mean local stress of the chain introduced in Sec. IV. Shock waves are possible only if the local stress of the chain is unequal to zero.

It is expected that the SOC attractor is a critical state in the sense that, on average, perturbations (i.e., avalanches) are *just* able to propagate through the whole system [5]. In the sandpile metaphor the slope of the pile is the dynamical "control parameter" which moves into the critical point. The corresponding, self-organizing "control parameter" in our model is the *Peierls barrier* of the shock waves, which they experience because of the discreteness of the chain. The barrier height is proportional to the strength of the external potential b, it decreases with increasing local stress $\bar{f}$, and it shrinks to zero for $\bar{f} \to b$ which corresponds to the stable stationary state with the largest energy. It is difficult to quantify the barrier height. Instead, we use the mean local stress $\bar{f}$.

In order to understand why the Peierls barrier is the self-organized "control parameter" we introduce a much simpler model, where the barrier is a control parameter. The model is a single damped particle on a tilted "washboard:" the slope f of the washboard is the control parameter. There is also a barrier which decreases with increasing slope. Thus, the slope f corresponds to the mean local stress $\bar{f}$. Propagating particle means shock wave and pinned particle means stationary state. The key property of the washboard model and the FK model is the *bistability* between propagation and pinning due to *inertia*. Bistability is possible only if the control parameter is above a critical value f_c. The question is now: does the weakly driven FK model organize its "control parameter" (i.e., the mean local stress) in such a way

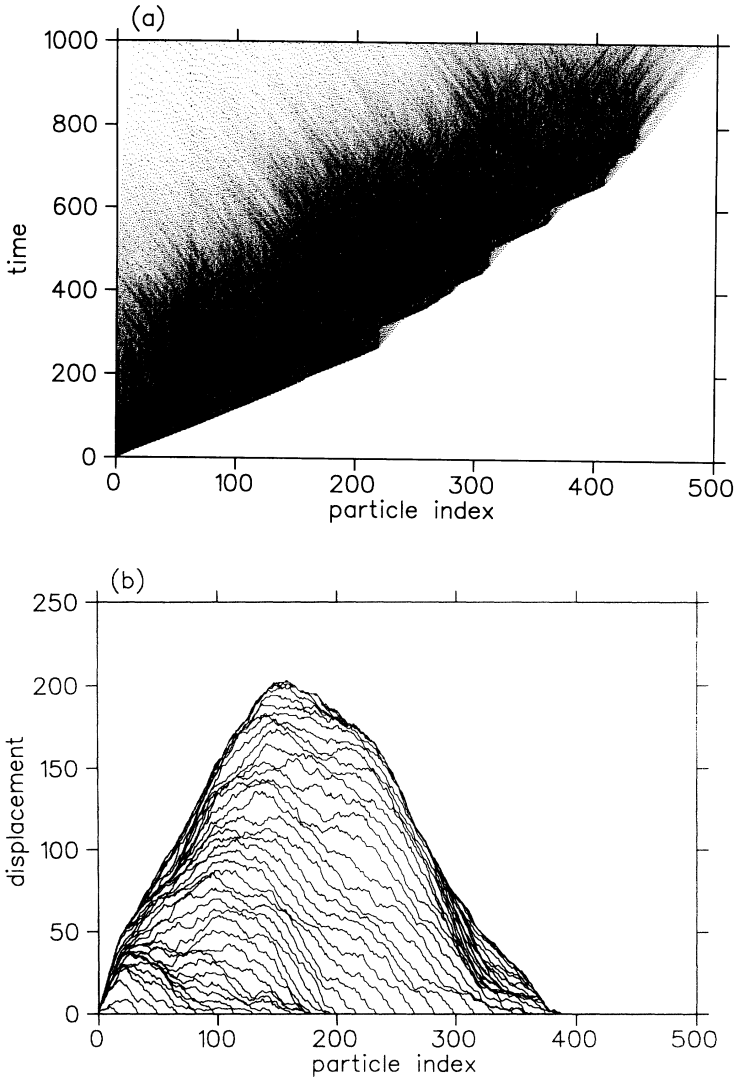

FIG. 12. A time-resolved single avalanche for $b = 1$, $N = 500$, and $g = 0.03$. Avalanche parameters: $\Delta E_{pot} = 2.65 \times 10^3$, $S = 4.37 \times 10^4$, $L = 386$, and $D = 1.05 \times 10^3$. (a) Density plot of the kinetic energy averaged over $2\pi/\sqrt{2b}$. (b) Displacement curves $x_i(t) - x_i(0)$ for equidistant time steps Δt with $\Delta t = 20$.

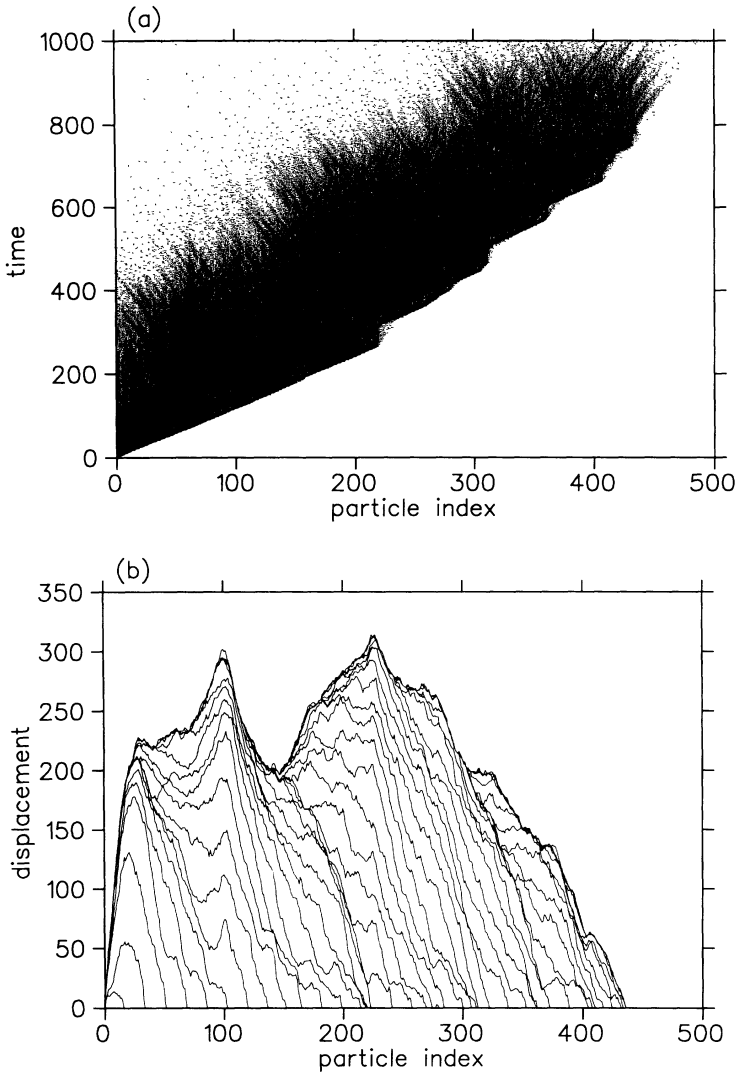

FIG. 13. A time-resolved single avalanche for $b = 5$, $N = 500$, and $g = 0.03$. Avalanche parameters: $\Delta E_{pot} = 1.67 \times 10^4$, $S = 8.96 \times 10^4$, $L = 435$, and $D = 9.45 \times 10^2$. (a) Density plot of the kinetic energy averaged over $2\pi/\sqrt{2b}$. (b) Displacement curves $x_i(t) - x_i(0)$ for equidistant time steps Δt with $\Delta t = 20$.

that $\overline{f} \approx f_c$, where an avalanche is just able to propagate through the whole chain?

In order to answer this question numerical experiments of the following type were done. A chain with 500 particles is prepared in a state with a periodic f-symbol sequence. The beginning of the chain (i.e., the first 15 particles) is "overloaded" which means that the mean local stress is much larger than for the rest of the chain. For the same initial state but varying damping constant g it is determined whether the avalanche propagates until the end of the chain or not. The experiments were done for $b = 1$. The f-symbol sequences were generated by a Markov process with transition probabilities derived from the distribution of two-symbol words taken from actual simulations for $g = 0.03$ and $g = 0.3$. The lengths of the f-symbol periods were 50 and 40, respectively. The experiments give clear evidence for the existence of a g_c with the property that for $g > g_c$ all avalanches always stop before reaching the end of the chain, and for $g < g_c$ they always reach the end. The filled squares and triangles in Fig. 14 show the relation between g_c and the mean local stress $\overline{f}$. The small fluctuations are caused by the fact that different f-symbol sequences with the same $\overline{f}$ may have slightly different Peierls barriers. Nevertheless we can draw a curve $f_c(g)$ through these points. Above this curve shock waves propagate. The open and larger squares in the figure denote the mean local stress from the SOC simulations. They lie directly on the curve. Therefore the FK model selects a mean local stress for which a perturbation is just able to propagate through the whole chain.

VII. THE TRANSITION TO REGULAR BEHAVIOR

For large g the SOC behavior will eventually disappear and regular behavior takes place. It is characterized by periodic orbits where always the same states periodically reappear, only shifted by some integer amounts of the periodicity of the external potential. The simplest orbit has period 1, and the avalanche is a single shock wave propagating from the pulled end to the free end of the chain. Orbits with higher periods contain at least one avalanche with $L = N$. Typically a large avalanche is accompanied by very small ones ($L < 10$).

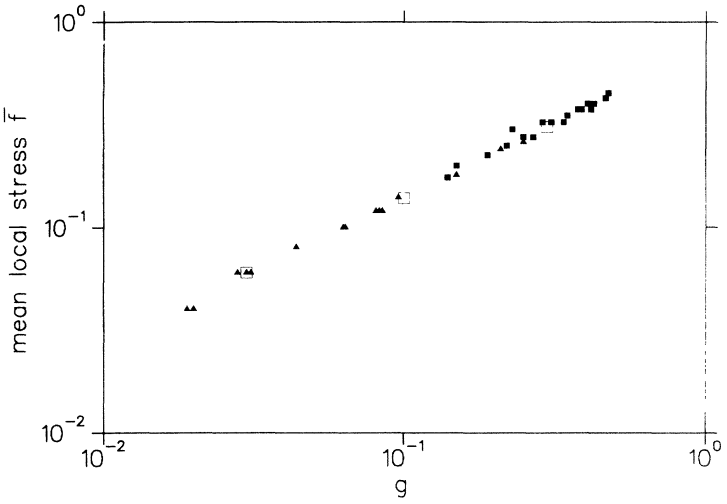

FIG. 14. Bistability regime of shock waves (filled symbols) and self-organized mean local stress (open squares) for $b = 1$. Filled squares and triangles denote the bistability edge for different states with periodic f-symbol sequences generated from two-symbol distributions taken from simulations with $g = 0.3$ and $g = 0.03$, respectively (for more details, see text).

There is no sharp transition from regular to irregular behavior. For example, for $b = 1$ and $N = 125$ period-2 orbits were found for $g = 0.28$ and $g = 0.4$, whereas for $g = 0.9$ in a particular simulation no periodicity was found after 2×10^4 avalanches. Thus, there is a broad transition regime ($g \approx 0.28$–0.95 for $b = 1$) of coexistence of regular and irregular behavior. There also is multistability between different periodic orbits. The number of periodic orbits and their basin of attraction (in the reduced phase space) seem to increase with g. It is difficult to decide whether an irregular orbit is indeed aperiodic (i.e., having a period comparable to the recurrence time) or whether it is only a transient. The avalanche statistics of the irregular cases deviate from the behavior shown in Sec. V. The degree of deviation increases with g. For $g = 0.9$ the distribution of the large avalanches show an exponential law instead of a power law. One reason may be an *intermittent* behavior where the erratic sequence of avalanches is interrupted by a regular episode of the following type: similar to the periodic case, one large shock wave travels through the chain up to a certain point and shifts all particles by the same integer amount. The stopping point comes nearer and nearer to the beginning of the chain from avalanche to avalanche. The regular episodes last at most until the stopping point reaches the beginning of the chain. Again these large avalanches may be accompanied by tiny ones.

In order to understand the behavior in this transition regime we look again at the single avalanche dynamics. Figure 15 shows an example for $g = 0.9$. The sound waves are nearly suppressed, and only shock waves are visible. At certain points they stop, change their direction of propagation, or split into two waves. The f-symbol sequence of the initial state of this particular example is the periodic pattern $\{0,1,0,1,\ldots\}$ with some imperfections. For example, around $i = 35$ it is changed into $\{\ldots,0,1,0,1,1,0,1,1,0,0,1,0,1,\ldots\}$. At that imperfection the initial shock wave splits into two waves [see Fig. 15(a)]. Before it reaches the splitting point it shifts each particle by unity [see Fig. 15(b)]. A similar shift happens during the propagation of the backward traveling wave.

We conclude from the inspection of Fig. 15(b) that almost all shock waves are *regular*, although the overall dynamics may be irregular. There are two types of regular shock waves. The first type turns a regular state (represented by a periodic f-symbol sequence) into the same state with the same f-symbol sequence only shifted by an integer. The other type turns a regular state into another regular one with a different f-symbol sequence but the same mean local stress. Regular shock waves are periodic solutions of the equation of motions (1) with given boundaries for $i \to \pm\infty$. For example, a shock wave of the first type which shifts the state $\{\ldots,1,1,1,\ldots\}$ by unity is given by $x_i(t) = n_i + x^{(0)} + \xi(i - ct)$, where $x^{(0)} = (1 - 1/b)/2$, c is the velocity, and ξ is a solution of the delay-differential equation

$$c^2\ddot{\xi}(t) - cg\dot{\xi}(t) = \xi(t+1) + \xi(t-1) - 2(1+b)\xi(t) + 2b\,\Theta(\xi(t) - 1 + x^{(0)}), \tag{26}$$

where Θ is Heaviside's step function. The boundary conditions are $\xi(t \to \pm\infty) = (1 \pm 1)/2$. Such a regular shock wave is possible only if (26) has a solution. Any regular shock wave is a solution of a similar boundary value problem of a delay-differential equation (or a set of them). If g is larger than a critical value g_c the boundary value problem will only have a solution for $c = 0$, i.e., a stationary kinklike structure. This is the same g_c as in Sec. VI.

Instead of solving such boundary value problems, numerical studies were performed by preparing both halves of the chain in the states defined by the boundary conditions. In the case of regular shock waves, the interface in the middle of the chain evolves into a single, confined shock wave if g is just below g_c. The state behind the shock wave may not be the same as given by the boundary values if the shock wave is of type 2. We found a second critical value $g_c^r < g_c$ below which the regular shock wave turns into an irregular one. An irregular shock wave is distinguished from a regular one by the fact that the particles behind it do not relax into a regular state. Instead they move further than is necessary to build up a state with same mean local stress as before the shock

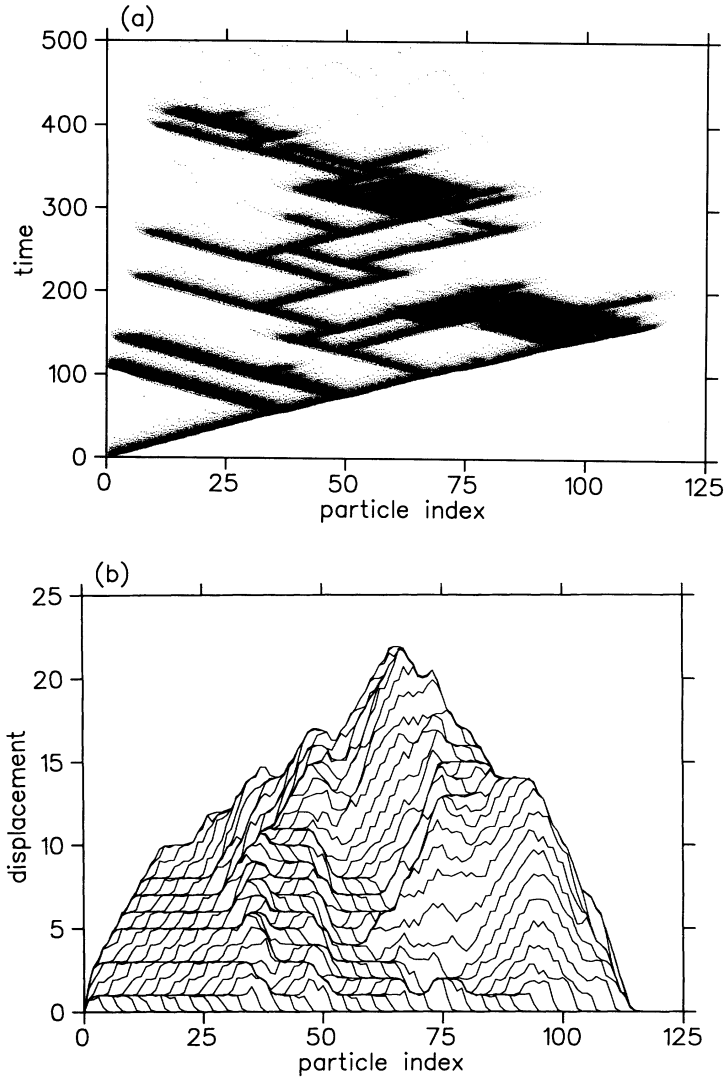

FIG. 15. A time-resolved single avalanche for $b = 1$, $N = 125$, and $g = 0.9$. Avalanche parameters: $\Delta E_{pot} = 7.89 \times 10^2$, $S = 1.47 \times 10^3$, $L = 113$, and $D = 4.19 \times 10^2$. (a) Density plot of the kinetic energy averaged over $2\pi/\sqrt{2b}$. (b) Displacement curves $x_i(t) - x_i(0)$ for equidistant time steps Δt with $\Delta t = 5$.

wave. This motion caused by inertia tends to decrease the mean local stress. Usually additional shock waves will be generated, some propagating backward, some forward but delayed. The state behind the initial shock waves become unpredictable although the initial state is regular. From the numerical experiments it is not possible to decide whether the irregular shock waves are caused by an instability or by the disappearance of the regular ones. Almost all shock waves in Figs. 12 and 13 are of the irregular type.

From Sec. VI we already know that g_c is a monotonically increasing function of the mean local stress $\bar{f}$. The same property holds for g_c^r. Numerical observations lead to the conjecture that regular shock waves are not possible (i.e., $g_c^r = g_c$) for mean local stresses below a critical value $\bar{f}_c$. The corresponding value of g_c where this happens defines the lower bound of the transition regime g_T^{low}. Thus for $g < g_T^{low}$ the inherent chaotic behavior of the irregular shock waves prevents the dynamics in the reduced phase space from becoming regular. The irregular behavior for $g > g_T^{low}$ is caused either by irregular shock waves or by irregularities of the initial state. These irregularities are unavoidable even for regular initial states because they are generated by the regular shock waves at boundaries. But a careful construction of the initial states makes it possible to find small periodic orbits in the reduced phase space even for very low values of g. The above mentioned orbits for $g = 0.28$ and $g = 0.4$ were constructed in this way. The f-symbol sequences are $\{(0,0,1)^2, (0,0,0,1,0,0,1)^{17}\}$ and $\{(0,0,1)^{41}, 0, 1\}$, respectively [27]. The other parameters are $a = 1.3$, $b = 1$, and $N = 125$. These orbits will be stable if the parameters of the systems are changed only slightly. But they are unstable if only one symbol is changed.

There seems to be no clear definition for the upper bound of the transition region. With increasing g the probability for irregular shock waves is reduced eventually to zero. But as mentioned above this does not exclude irregular behavior. The following observation may be important: for $b = 1$ and $g = 0.95$ a huge number of states (but not all) of the form $\{(1,0)^{m_1}, 1, (1,0)^{m_2}, 1, \ldots, (1,0)^{m_M}, 1, 1\}$ are reproduced by an orbit of period 1 or 2. Thus, the upper bound may be defined by the point where an *irregular* state is reproduced by a *regular* shock wave.

VIII. CONCLUSION

In this paper the self-organization due to weak local driving (i.e., slow pulling of one end of the chain) of the damped FK model with a piecewise parabolic potential was studied in detail. The piecewise parabolic potential makes it possible to drive the system infinitesimally slowly because stability intervals of all stationary states are computable. Therefore, as in "sandpile" models, a separation of the dynamics between driving (putting the system at the edge of the instability) and relaxing due to an avalanche is possible.

The driving mechanism leads to an attractor which is characterized by the fact that, on average, the difference between successive springs (i.e., $x_{i+1} - 2x_i + x_{i-1}$) called local stress is equal for each particle in the bulk of the chain. The mean local stress corresponds to the mean slope of a sandpile. And, as in those "sandpile" models, it also organizes itself into a critical state where a perturbation is just able to propagate through the whole chain. The mean local stress is the self-tuned "control parameter" of the system, because particle hopping releases energy by reducing local stress. The released energy drives shock waves of particle-hopping events which build up avalanches. The mean local stress of the chain has the same effect as a constant externally controlled force applied to each particle. The coexistence between propagation and pinning due to inertia is responsible for SOC.

The chain must be relatively long ($N > 125$) in order to get power laws of the distributions of avalanche strengths and lengths. The weaker the potential the longer it must be. The discreteness of the model means that SOC is a statistical property clearly visible only in the thermodynamic limit. We have measured the cumulative distributions of the avalanche strength calculated either by the energy drop ΔE_{pot} or by the displacement sum S (in almost all cases S/N is the displacement of the center of mass). In both cases the exponent is roughly 1/2, whereas it is roughly 1 for the avalanche length. We have also measured the power spectra of the fluctuating pulling force. The exponent increases from 1 to 2 with decreasing damping constant.

If dissipation is strong enough the irregular behavior of the SOC regime will turn into a regular one. In the regular regime a sequence of states reappears periodically, only rigidly shifted by an integer multiple of the periodicity of the external potential. The transition between irregular and regular behavior is relatively broad. It is characterized by the coexistence between irregular behavior and several periodic orbits. In the irregular case the type of avalanche distribution changes smoothly from a power law at the lower edge of the transition regime to an exponential law at the upper edge. The irregular non-SOC behavior is accompanied by a kind of intermittency.

As mentioned in the Introduction, the FK model is very similar to the BK model and in fact it becomes the BK model for $b \to \infty$. In [15] the BK model was also driven by slow pulling of one end of the chain (train model). The exponents of the power laws of the avalanche distributions are in good agreement with our results from the FK model. Preliminary simulations have shown that we also get similar results as in [12,13] if the FK model is driven like the BK model in those papers (i.e., all particle are connected with a slowly moving rigid plate via soft springs). In particular, the same kind of phase transition as in [13] occurs if the friction parameter is varied. In [13] it is argued that in such uniformly driven BK models criticality needs some fine tuning rather than being self-organized.

In [9] the FK model was also driven by slowly pulling one end of the chain. But the external potential was given by randomly distributed pinning centers, and the dynamics was a kind of overdamped dynamics. That is, instead of simulating the avalanche dynamics the next state was chosen by the rule to take the state with the smallest shift of the center of mass. The distribution of avalanche strength measured by the energy drop gives a power law with an exponent of roughly 0.8, i.e., half of the value we obtained. The distributions of the center-of-mass displacements do not show any power law. The power spectra of the pulling force shows a $1/f^{1.5}$ law which is roughly similar to our results.

Concerning the conditions for SOC there remain a number of open questions. (i) What is the role of a random external potential? (ii) What are the effects of different types of driving (uniform versus nonuniform, reducing the number of metastable states versus leaving it constant)? (iii) For which kind of models is inertia important? (iv) What is the role of the dimensionality of the model?

Another important and open question not concerning SOC is: what happens for finite pulling velocities? For small velocities avalanching will still be the dominant behavior as long as the averaged waiting time between successive avalanches is smaller than the averaged avalanche duration. For larger velocities the chain will never be at rest. For small values of the damping constant phonon resonances are expected [28]. For very large velocities a strong damping force will dominate the force from the external potential. Thus we expect the same behavior mentioned in Sec. IV, paragraph 7.

ACKNOWLEDGMENTS

I gratefully acknowledge helpful discussions with T. Christen, S. Fauve, J. Langer, R. Schilling, M. de Sousa Vieira, T. Strunz, H. Suhl, P. Talkner and H. Thomas. I also acknowledge the possibility of doing the simulations on the NEC SX-3 at the Centro Svizzero di Calcolo Scientifico at Manno, Switzerland. This work was supported by the Swiss National Science Foundation.

[1] Y.I. Frenkel and T. Kontorova, Zh. Eksp. Teor. Fiz. **8**, 1340 (1938).
[2] S. Aubry, in *Solitons in Condensed Matter Physics*, edited by A.R. Bishop and T. Schneider (Springer-Verlag, New York, 1978); P. Bak, Rep. Prog. Phys. **45**, 587 (1982).
[3] L. Pietronero, W.R. Schneider, and S. Strässler, Phys. Rev. B **24**, 2187 (1981); F. Vallet, R. Schilling, and S. Aubry, Europhys. Lett. **2**, 815 (1986).
[4] C. Tang, K. Wiesenfeld, P. Bak, S. Coppersmith, and P. Littlewood, Phys. Rev. Lett. **58**, 1161 (1987); S.N. Coppersmith, *ibid.* **65**, 1044 (1990); A.A. Middleton and D.S. Fisher, *ibid.* **66**, 92 (1991).
[5] P. Bak, C. Tang, and K. Wiesenfeld, Phys. Rev. Lett. **59**, 381 (1987).
[6] P. Bak, C. Tang, and K. Wiesenfeld, Phys. Rev. A **38**, 364 (1988); P. Bak and C. Tang, J. Geophys. Res. B **94**, 15 635 (1989); L.P. Kadanoff, S.R. Nagel, L. Wu, and S. Zhou, Phys. Rev. A **39**, 6524 (1989); H. Nakanishi, *ibid.* **41**, 7086 (1990); X. Che and H. Suhl, Phys. Rev. Lett. **64**, 1670 (1990).
[7] F.J. Elmer, Helv. Phys. Acta **66**, 99 (1993).
[8] F.J. Elmer, Europhys. Lett. **20**, 363 (1992).
[9] H.J. Jensen, Y. Brechet, and B. Doucot, J. Phys. I (France) **3**, 611 (1993).
[10] O. Pla and F. Nori, Phys. Rev. Lett. **67**, 919 (1991).
[11] R. Burridge and L. Knopoff, Bull. Seismol. Soc. Am. **57**, 341 (1967).
[12] J.M. Carlson and J.S. Langer, Phys. Rev. Lett. **62**, 2632 (1989); Phys. Rev. A **40**, 6470 (1989); D. Sornette, J. Phys. I (France) **2**, 2089 (1992).
[13] G.L. Vasconcelos, M. de Sousa Vieira, and S.R. Nagel, Physica A **191**, 69 (1992); M. de Sousa Vieira, G.L. Vasconcelos, and S.R. Nagel, Phys. Rev. E **47**, R2221 (1993).
[14] L. Knopoff, J. A. Landoni, and M.S. Abinante, Phys. Rev. A **46**, 7445 (1992).
[15] M. de Sousa Vieira, Phys. Rev. A **46**, 6288 (1992).
[16] D.S. Fisher, Phys. Rev. B **31**, 1396 (1985).
[17] D.P. Vallette and J.P. Gollub, Phys. Rev. E **47**, 820 (1993).
[18] If the cusps of the external potential were slightly rounded the jumps would be replaced by curves of unstable states connecting the pieces of stable states. Thus the end points of the stable pieces are related to saddle-node bifurcations.
[19] S. Aubry, J. Phys. C **16**, 2497 (1983).
[20] A.J. Lichtenberg and M.A. Lieberman, *Regular and Stochastic motion* (Springer-Verlag, New York, 1983).
[21] W. Kob and R. Schilling, Phys. Rev. A **42**, 2191 (1990).
[22] D.W. Heermann, *Computer Simulation Methods in Theoretical Physics* (Springer-Verlag, Berlin, 1986).
[23] G.S. Grest, C.M. Soukoulis, and K. Levin, Phys. Rev. Lett. **56**, 1148 (1986).
[24] W. Kob and R. Schilling, J. Phys. A **23**, 4673 (1990).
[25] H.J.S. Feder and J. Feder, Phys. Rev. Lett. **66**, 2669 (1991); **67**, 283(E) (1991).
[26] S. Ciliberto and C. Laroche, J. Phys. I (France) **4**, 223 (1994).
[27] Exponentiation denotes repetition of the sequence in parentheses.
[28] S. Aubry and L. de Seze, Festkörperprobleme **25**, 59 (1985).

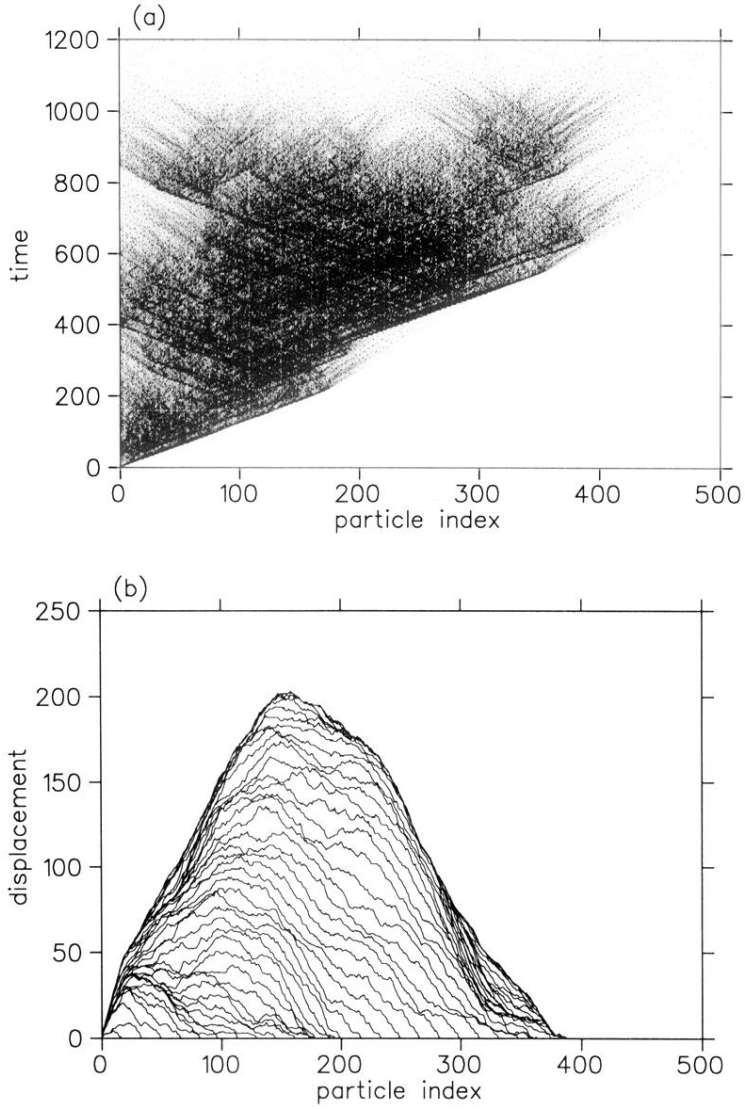

FIG. 12. A time-resolved single avalanche for $b = 1$, $N = 500$, and $g = 0.03$. Avalanche parameters: $\Delta E_{pot} = 2.65 \times 10^3$, $S = 4.37 \times 10^4$, $L = 386$, and $D = 1.05 \times 10^3$. (a) Density plot of the kinetic energy averaged over $2\pi/\sqrt{2b}$. (b) Displacement curves $x_i(t) - x_i(0)$ for equidistant time steps Δt with $\Delta t = 20$.

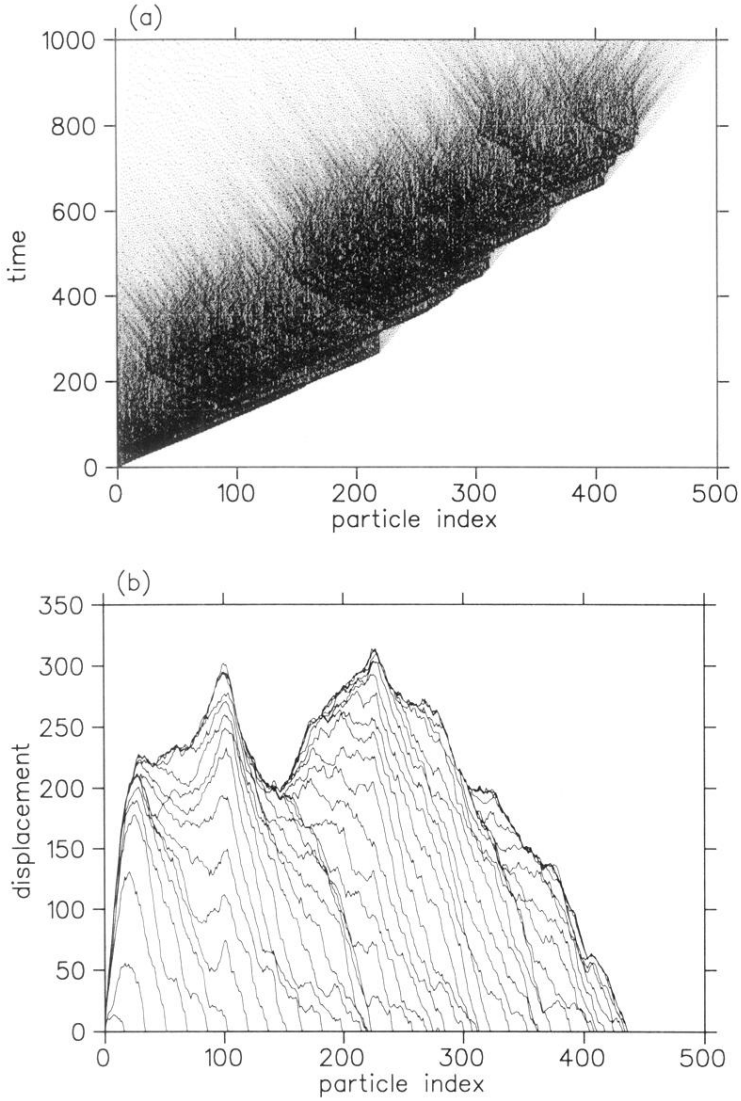

FIG. 13. A time-resolved single avalanche for $b = 5$, $N = 500$, and $g = 0.03$. Avalanche parameters: $\Delta E_{pot} = 1.67 \times 10^4$, $S = 8.96 \times 10^4$, $L = 435$, and $D = 9.45 \times 10^2$. (a) Density plot of the kinetic energy averaged over $2\pi/\sqrt{2b}$. (b) Displacement curves $x_i(t) - x_i(0)$ for equidistant time steps Δt with $\Delta t = 20$.

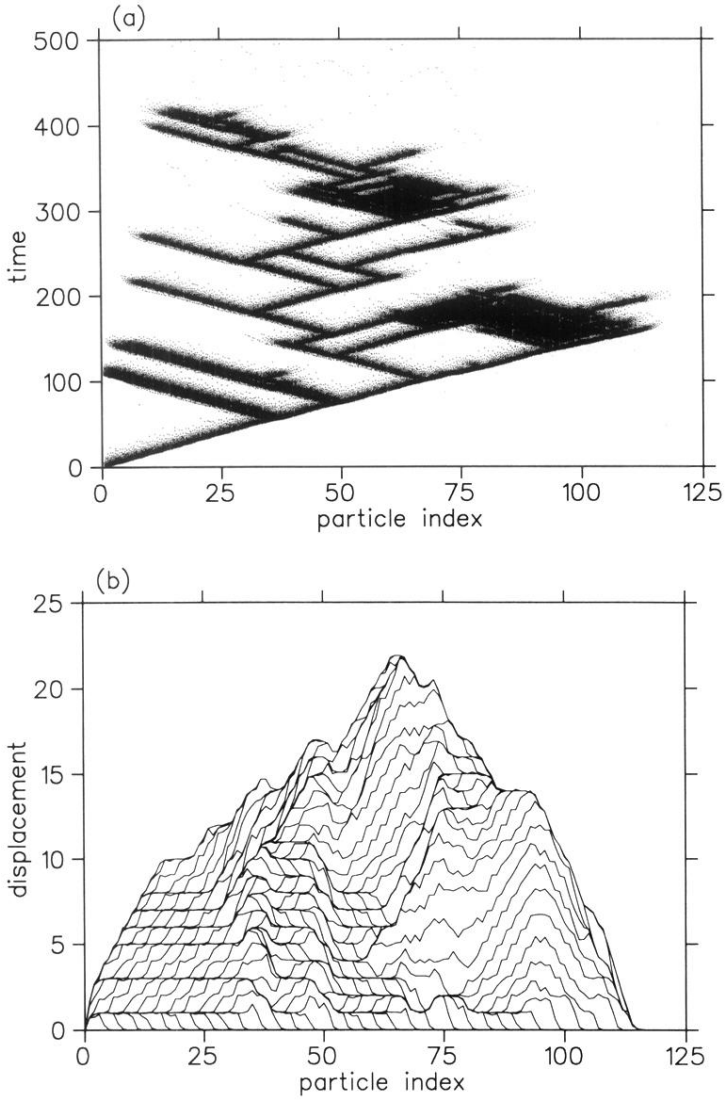

FIG. 15. A time-resolved single avalanche for $b = 1$, $N = 125$, and $g = 0.9$. Avalanche parameters: $\Delta E_{pot} = 7.89 \times 10^2$, $S = 1.47 \times 10^3$, $L = 113$, and $D = 4.19 \times 10^2$. (a) Density plot of the kinetic energy averaged over $2\pi/\sqrt{2b}$. (b) Displacement curves $x_i(t) - x_i(0)$ for equidistant time steps Δt with $\Delta t = 5$.